Applied Catalysis B: Environmental 138–139 (2013) 285–293

Contents lists available at SciVerse ScienceDirect

Applied Catalysis B: Environmental

journal homepage: www.elsevier.com/locate/apcatb

Silver palladium core–shell electrocatalyst supported on MWNTs for ORR in alkaline media

Ryan C. Sekol, Xiaokai Li, Peter Cohen, Gustavo Doubek, Marcelo Carmo[1], André D. Taylor*

Chemical and Environmental Engineering Department–Yale University, 9 Hillhouse Ave, New Haven, CT, 06511, USA

ARTICLE INFO

Article history:
Received 14 September 2012
Received in revised form 22 February 2013
Accepted 25 February 2013
Available online 6 March 2013

Keywords:
Oxygen reduction reaction
Electrocatalysts
Core–shell catalyst
Alkaline fuel cells
Direct alcohol fuel cells

ABSTRACT

We show that silver palladium core-shell catalysts supported on multiwalled carbon nanotubes (Ag@Pd/MWNTs) are highly active and alcohol tolerant for oxygen reduction reactions (ORR) in alkaline media. These electrocatalysts were synthesized by galvanic displacement of Pd on Ag nanoparticles deposited on MWNTs. The Ag@Pd/MWNTs are shown to be tolerant of the presence of methanol and ethanol in the electrolyte. In the presence of methanol, the Ag@Pd/MWNTs current density decreased by 0.18 mA/cm^2, compared to Pt/C (0.97 mA/cm^2) and Pd/C (1.09 mA/cm^2). In the presence of ethanol, the Ag@Pd/MWNTs current density decreased by 0.12 mA/cm^2, compared to Pt/C (0.87 mA/cm^2) and Pd/C (2.13 mA/cm^2). The Ag@Pd/MWNTs also show improved durability with an increased mass activity of ~3.5 times that of standard Pd/C, after durability testing in ethanol. The Ag@Pd/MWNTs are promising platinum free direct alcohol fuel cell cathode catalysts due to their high activities and durability, as well as their improved tolerance to methanol and ethanol from possible fuel crossover.

1. Introduction

Recent advances in polymer anion exchange membranes have led to increasing studies of alkaline fuel cells (AFCs) [1–3]. AFCs have advantages over traditional proton exchange membrane fuel cells (PEMFCs) due to improved kinetics in the alkaline media where transition metals that are cheaper than Pt can be used without a significant penalty in activity [4]. Previous studies have shown that palladium can be used as an anode catalyst [5] and silver as the cathode catalyst [6,7]. Although low anodic overpotentials facilitate alcohol oxidation in alkaline media, the slow kinetics of the oxidation reduction reaction (ORR) remains a significant challenge [4,7]. Silver is a promising replacement for platinum because it has similar mechanisms and kinetics for ORR catalysis [8]. Ag has a higher tolerance toward methanol poisoning than Pt [6]. In addition, Ag rapidly decomposes hydroxide ions [9], that can form peroxides known to cause membrane degradation. While no single metal catalyze the ORR as effectively as Pt [10], it has been suggested that the higher Ag overpotential could be reduced by alloying Ag with other selected metals [7].

Core–shell catalysts are being increasingly used for bi-metallic catalysts due to the enhanced catalytic activity produced through electronic modification of the bimetallic structure [11–13]. This enhancement is caused by the ligand effect which changes the d-band position, and affects the adsorption, activation energies, and charge transfer [13–15]. The core–shell structure also optimizes the utilization of expensive metals in the shell, helping to reduce cost [16]. As an example, it has been shown that a PtFe shell with a Pd core catalyst has a current density ~12 times higher and a more positive onset potential (140 mV) compared to a commercial Pt/C (ETEK) catalyst in an acidic media. This effect is due to the interfacial interactions between the thin shell and core [12]. It has been suggested that the structure of the core–shell catalyst increases durability due to the decreased metal segregation of the catalyst [17]. Previously, a Ag@Pd catalyst was shown to increase the atom-efficiency of Pd, while also enhancing the selectivity of hydrogenation due to the sub-surface Ag [18]. The increase in atom-efficiency is due to the Pd surface dissociating the hydrogen and catalyzing the reaction and the Ag preventing hydrogen migration into the core of the particle [19]. Recently, it has also been shown that Ag@Pd/C catalyst is tolerant to alcohol present during ORR in alkaline conditions with similar activity as Pt/C [20]. While these promising Ag@Pd catalyst systems were mostly studied on amorphous carbon supports or free standing nanoparticles, there has not been any report comparing these materials on highly active

* Corresponding author at: P.O. Box 208286, New Haven, CT 06520-8286, USA. Tel.: +1 203 432 2217; fax: +1 203 432 4387.
E-mail addresses: ryan.sekol@yale.com (R.C. Sekol), xiaokai.li@yale.edu (X. Li), peter.g.cohen@yale.edu (P. Cohen), gustavo.doubek@yale.edu (G. Doubek), m.carmo@fz-juelich.de (M. Carmo), andre.taylor@yale.com (A.D. Taylor).
[1] Present Address: Forschungszentrum Jülich GmbH – Institute of Energy and Climate Research, Wilhelm-Johnen-Straße, Jülich, 52428 – Germany.

0926-3373/$ – see front matter © 2013 Elsevier B.V. All rights reserved.
http://dx.doi.org/10.1016/j.apcatb.2013.02.054

1-D carbon supports. The use of 1-D carbon supports such as carbon nanotubes has previously produced more active catalysts due to increased surface area, conductivity, and stability of the support [21–25].

In this work we present a silver palladium core shell catalyst supported on multiwalled carbon nanotubes (MWNTs) as an effective ORR catalyst. The core shell structure was synthesized using galvanic displacement of Ag supported on MWNTs with Pd. The Ag@Pd/MWNT catalyst system was investigated for ORR activity and tolerance of alcohols during ORR (simulating alcohol crossover) and compared with commercial Pt/C and Pd/C catalysts in terms of activity and durability.

2. Experimental

2.1. MWNT functionalization

In a 500 mL flask equipped with a condenser, 6.0 mg of pristine MWNTs (SWeNTs Inc.), HNO_3 (65%, 50 mL), and H_2SO_4 (98%, 150 mL) were added with vigorous stirring. The flask was then immersed in an ultrasonic bath for 10 min. The mixture was then stirred for 100 min under reflux (oil bath temperature was increased gradually from 90 to 133 °C). A dense brown gas was evolved during this period, which was collected and treated with aqueous NaOH. After cooling to room temperature, the reaction mixture was diluted with 250 mL of deionized water (DI) and then vacuum-filtered through a 0.2 μm filter paper. The solid was dispersed in 250 mL of DI water and filtered again, and then 200 mL of DI water was used to wash the filter cake several times. The dispersion, filtering, and washing steps were repeated until the pH of the filtrate reached 7. The filtered solid was then dried under vacuum for 24 h at 60 °C.

2.2. Silver nanoparticle decoration

For decoration of MWNTs, a 100 ml flask containing 20 ml of DI water and 10 mg of oxidized MWNT were dispersed in an ultrasonic bath for 3 min and then the flask was placed on a magnetic stirrer. With stirring at room temperature, an aqueous silver nitrate solution (20 ml, 0.01 M) was added drop-wise into the flask. After 20 h of continuous stirring, the solid product (Ag/MWNT) was then collected by filtration. The decoration of carbon black was based on previous work done in the literature [26]. 100 mg of carbon black and 40 mg of silver nitrate were dry mixed with a mortar and pestle until the mixture was homogenous. The powder was then transferred to a quartz boat and placed in a tube furnace. The furnace was heated to 450 °C under a nitrogen atmosphere for 3 h with a 5 degree/min ramp rate.

2.3. Silver displacement

A 0.8 mM solution of $PdCl_2$ (Sigma–Aldrich) was prepared in 20 mL of DI water, and was then sonicated for 1 h. Concurrently with the sonication, a 10 μL drop of the Ag/MWNTs or Ag/C ink was deposited on a glassy-carbon electrode, with a Ag loading of 25 $\mu m/cm^2$, and then left to dry in ambient conditions. After the sonication of the 0.8 mM Pd solution, the displacement of Ag with Pd took place in a 30 mL beaker with a Pt mesh counter-electrode and Ag/AgCl reference electrode. The open circuit voltage (OCV) was measured using the electrochemical measurement set-up described below.

2.4. Physical catalyst characterization

Thermogravimetric analysis (TGA), using a TA Instruments Q50 analyzer, was used to determine the actual loading of the prepared catalysts as described previously [27]. In brief, experiments were conducted by increasing the sample temperature to 800 °C in air. Catalyst loadings were calculated based on the initial mass of the silver–carbon (Ag/MWNTs) nanocomposite and the final mass of the remaining Ag_2O particles. To determine the ratio of palladium and silver present in the core–shell particles inductively coupled plasma (ICP) measurements were conducted using a PerkinElmer Elan DRC-e inductively coupled plasma mass spectrometer (ICP-MS). Transmission electron microscopy (TEM) was performed using a FEI Tenai Biotwin 120 kV high-resolution electron microscope to determine particle size and dispersion on the support, while Energy-dispersive spectroscopy (EDS) was carried out on a FEI Tecnai Osiris 200 kV TEM to determine the core–shell structure of the catalyst.

2.5. Electrochemical measurements

The electrochemical measurements were conducted in an electrochemical cell from PINE Instruments using a glassy carbon rotating disk electrode (RDE) set up with a multichannel potentiostat (Bio-Logic Instruments) and rotation control (AFR, Pine Instruments). Testing was conducted using a standard 3 cell set-up with a Pt mesh counter electrode and a Hg/HgO (MMO) reference electrode. Cyclic voltammetry (CV) characterizations were performed on the working electrodes by cycling the voltage between −0.9 and 0.3 V versus MMO at 50 mV/s in nitrogen purged 1 M KOH solution at room temperature. For the oxidation reduction reaction (ORR), the electrolyte was bubbled for 30 min with oxygen gas. Linear sweep voltammograms were done at 400, 625, 900, 1600, and 2500 RPM with a scan rate of 5 mV/s. To evaluate the alcohol crossover tolerance of the electrocatalysts, solutions of 1 M KOH and either 1 M methanol or 1 M ethanol were used as the electrolyte for ORR testing. The same procedure was used as stated above except, the KOH solution was removed and replaced with either the methanol or ethanol solution before the oxygen saturation process. Durability of the catalysts was determined by chronoamperometry in O_2 saturated electrolyte at 1600 RPM for 30 min with the potential fixed at −0.1 V vs MMO [20]. For all electrochemical testing a catalyst ink formation was created and 10 μL of solution was dried on a glassy carbon electrode (GCE). The ink solution was formulated to deposit 25 $\mu g/cm^2$ of metal on the GCE. For the displacement methods, a 10 μl drop of Ag/MWNTs was placed onto a glassy carbon electrode with a loading of 25 $\mu m/cm^2$ [6,7]. After the drop dried, the electrode was placed into the displacement solution and the open circuit voltage (Fig. 3) was monitored to determine the progress of the reaction. Once the OCV reached a steady state potential, the reaction was stopped by removing the electrode from the solution and rinsing with DI water.

3. Results and discussion

3.1. Verification of Pd displacement of Ag/MWNTs

The core–shell catalysts were synthesized by first depositing silver nanoparticles on the surface of the carbon support (described previously [26]), followed by galvanic displacement with palladium. The galvanic displacement with Pd is a self-terminating process that creates a thin shell of Pd on the surface of the Ag nanoparticles. Fig. 1 shows the CVs of the Ag/MWNTs before and after the displacement with Pd. During the forward scan, a peak is observed between 0.2 and 0.3 V, which correlates to the formation of Ag_2O on the Ag/MWNTs catalyst surface. The silver loading was determined to be 14 wt.% on the MWNTs. The Ag_2O is then reduced during the reverse scan with a sharp peak at 0.2 V. For the Ag@Pd/MWNTs catalyst, the silver oxide reduction peak is not

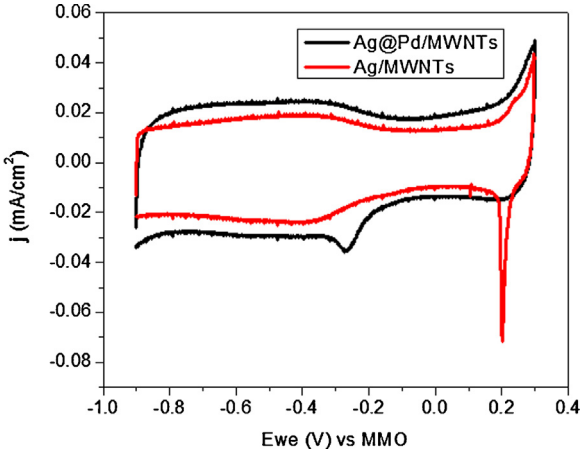

Fig. 1. CV in 1 M KOH saturated with N_2 and 50 mV/s scan rate.

present around 0.2 V and instead occurs as a broad peak at −0.29 V. Based on these observations, we suggest there is no significant amount of Ag present on the surface of the Ag@Pd particles. We note that Jiang et al. previously studied Ag@Pd/C but did not completely displace the surface of the Ag particles as the peak at 0.2 V was still present [20].

Pd displaces the Ag due to the difference in standard potentials, as shown in the Eqs. (1–3). This overall increase in potential results in a spontaneous irreversible redox process of a Pd coating on the surface of the Ag particles [28]. We present TEM images to confirm the presence of the Ag@Pd core shell structure as opposed to Pd depositing on the surface of the carbon. Fig. 2A shows the Ag/MWNTs with average particle size of 4.4 nm prior to Pd displacement and Fig. 2B shows the Ag@Pd core shell structures on the surface of the MWNTs, with an average core shell size of 7.5 nm; the inset (Fig. 2D) displays the energy-dispersive spectroscopy (EDS) line scan taken of two core–shell particles and shows the presence of a Pd-rich layer on the surface of the Ag particle. We show via the TEM image (Fig. 2C) that the line scan verifies the formation of a core–shell nanoparticle structure, due to the overlap of the Ag and Pd counts over the particles. Inductively couple plasma (ICP) measurements confirm the ratio of metals by weight in the Ag@Pd/MWNTs is 20% Pd and 80% Ag.

$$Ag_{(s)} \rightarrow Ag^{+} + e^{-} \qquad E^{\circ} = -0.80\,V \qquad \text{eq. (1)}$$

$$Pd^{2+} + 2e^{-} \rightarrow Pd_{(s)} \qquad E^{\circ} = +0.92\,V \qquad \text{eq. (2)}$$

$$Ag_{(s)} + Pd^{2+} \rightarrow Ag^{+} + Pd_{(s)} \qquad E^{\circ} = +0.12\,V \qquad \text{eq. (3)}$$

3.2. Comparison of Pd displacement methods

We investigated the effect of pH and temperature on the electrochemical properties of the core–shell particles as these variables typically influence the galvanic displacement rate [11,20,28]. The displacement of Ag by Pd was done under three different conditions with an excess of Pd and the concentration of the solution held constant (0.8 mmol $PdCl_2$ in water) at either 25 °C, 40 °C, or with 50 mmol HNO_3 at 25 °C, in order to determine if the time for the displacement can be reduced and/or the quality of the Ag@Pd catalyst can be improved by increasing the kinetics of the displacement.

The displacement reaction was monitored by measuring the OCV and is complete when the OCV reaches a plateau (Fig. 3A). We were able to vary the rate of displacement by 37.5 min by adjusting the pH and temperature of the solution. The rate of displacement is increased by performing the reaction at lower pH with the fastest displacement method of 0.8 mmol $PdCl_2$ in 50 mmol HNO_3 solution at 25 °C taking only 16.5 min, whereas at higher pH the displacement took 54 min to complete. Increasing the temperature at which the displacement took place resulted in the displacement being completed by 19 min. After the displacement procedure, the catalyst was capped with 10 μl of Nafion solution to ensure the sample adhered to the GCE. Fig. 3B shows a comparison of the three different displacement procedures for ORR at 1600 rpm.

However, the faster displacement methods produce lower current densities at −0.1 V (Fig. 3B). The displacement at 25 °C has the highest current density of −0.40 mA/cm^2 at −0.1 V and is 0.07 mA/cm^2 (83.5%) higher in current density compared to the acidic displacement at the same temperature and is 0.17 mA/cm^2 greater than the 40 °C displacement. We note that the displacement at 25 °C also has the most positive onset potential of −0.079 V. The acidic displacement has a decrease of 4 mV, followed by the high temperature displacement onset potential which has a decrease of 12 mV from the 25 °C displacement. We speculate that the difference in current densities could be related to the surface area of the metal nanoparticles, the thickness of the Pd shell over the Ag core, or the differences in pH during the reduction of the Pd particles during displacement. From this point forward the displacement procedure used for the synthesis of the Ag@Pd/MWNTs was carried out at 0.8 mmol $PdCl_2$ in water at 25 °C. We note that we synthesized the Ag@Pd/C under these same conditions and has the same OCV displacement profile, which is not shown, as the Ag@Pd/MWNTs (Fig. 3A), with the precursor being 20 wt.% Ag/C.

Table 1
Koutecky–Levich slopes and average number of electron transferred.

Material	Average K–L slope	Average electron transferred
Pd/C	4.87	3.99
Pt/C	4.92	3.99
Ag/MWNTs	6.52	2.98
Ag@Pd/MWNTs	6.77	2.87
Ag/C	5.67	3.43
Ag@Pd/C	5.10	3.81

3.3. ORR measurements of Ag@Pd/MWNTs

The catalyst activity was determined by ORR measurements carried out in O_2 saturated 1 M KOH at 1600 RPM (Fig. 4). The onset potential for the Ag@Pd/MWNTs, −0.091 V is lower than Pt/C ETEK, 0.006 V, and Pd/C, −0.032 V. While the Ag@Pd/MWNTs do not have a higher current density in KOH at −0.05 V or −0.1 V compared to Pt/C ETEK and Pd/C (Fig. 4), we show a distinct advantage by comparing the mass activity of the core–shell catalyst in the presence of alcohols later in the manuscript.

The effect of the Ag@Pd core shell can be seen by looking at the current density in the mass transport limited regime at −0.4 V. The Ag@Pd/MWNTs catalyst has a current density of −5.6 mA/cm^2 and the Ag/MWNTs has a current density of −3.13 mA/cm^2, an improvement of 2.3 mA/cm^2. The Ag@Pd/C also has a higher current density (−5.22 mA/cm^2) than its core–shell precursor Ag/C (−2.56 mA/cm^2). While there is an increase in activity due to MWNTs being a more active support because of the high conductivity and available surface area [27], we show that the Ag@Pd/MWNTs having a greater current density is not just an effect of the carbon support.

To determine the kinetics of the ORR, Koutecky–Levich Plots (Fig. 5) show kinetics of the ORR summarized in Table 1 for the following catalysts: Ag@Pd/MWNTs, Ag/MWNTs, Pt/C, and Pd/C. Linear sweep voltammograms were taken at 400, 625, 900, 1600, and 2500 RPM and fitted to the Koutecky–Levich equation to determine the average number of electrons transferred during the ORR [7].

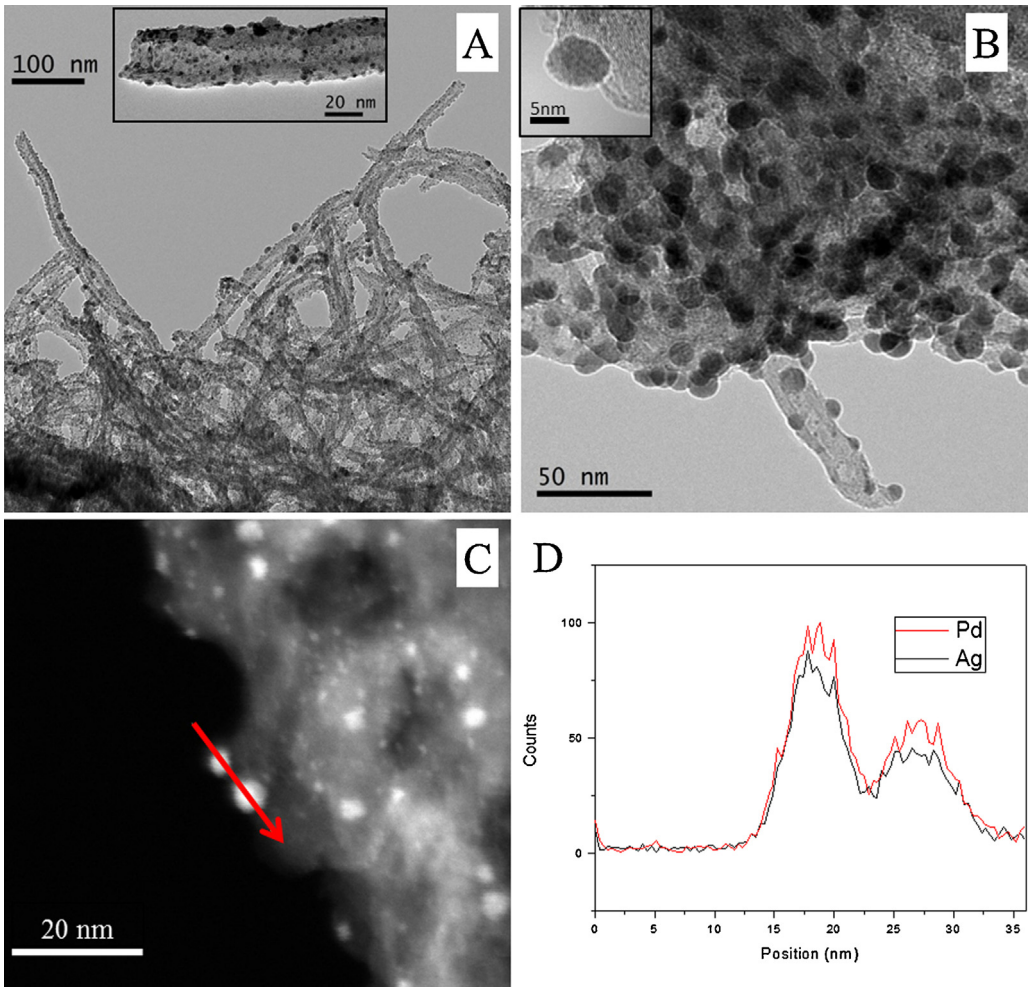

Fig. 2. Transmission electron microscopy images of A and Inset: Ag/MWNTs before Pd displacement, B: Ag@Pd/MWNTs (inset: single core–shell particle), C: HAADF image with arrow showing the location of the line scan D: EDX line scan of 2 Ag@Pd/MWNTs particles.

The Koutecky–Levich plots for all the catalysts show linear dependence at all three potentials. This linear and parallel plot indicates that these reactions have first order kinetics with respect to oxygen [7]. From the Koutecky-Levich plots, the average number of electrons transferred for the Pt/C ETEK and Pd/C are ~4, which corresponds to values typically found in literature [1,7,29]. The average number of electrons transferred for the Ag@Pd/MWNTs is ~3, with the core–shell precursor (Ag/MWNTs) also transferring an average of ~3 electrons. For the Ag@Pd/C catalyst the average number of electrons being transferred is 3.81 and the Ag/C also transfers 3.43 electrons, which is typical of Ag/C seen in literature (3.5–3.9 electrons transferred [6,7]). An average electron transfer of 4 electrons indicates the ORR is the 4-electron pathway, while an average electron transfer between 2 and 4 electrons indicates both the 2-electron (a two-step pathway with H_2O_2 produced as an intermediate and the rate determining step [20]) and

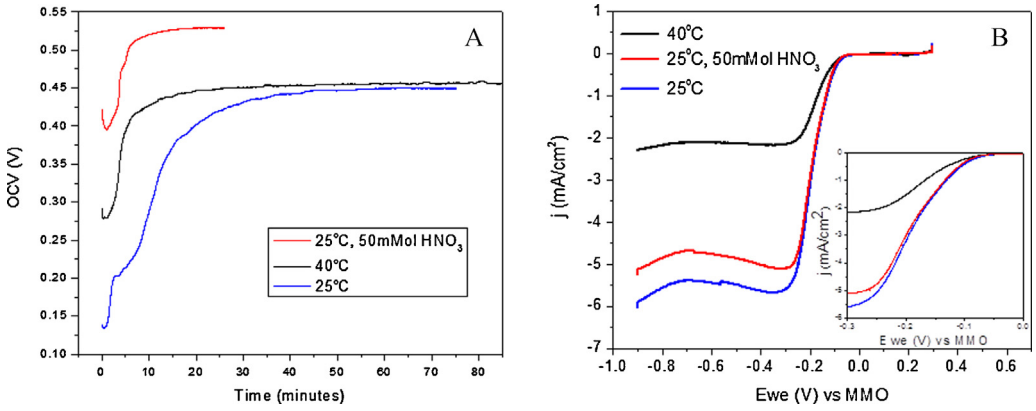

Fig. 3. A: The open circuit voltage measurement during three displacement procedures. B: Ag@Pd/MWNTs ORR at 1600 rpm in 1 M KOH saturated with O_2 with a 5 mV/s scan rate, comparing three displacement procedures, inset: expanded ORR curves around −0.1 V.

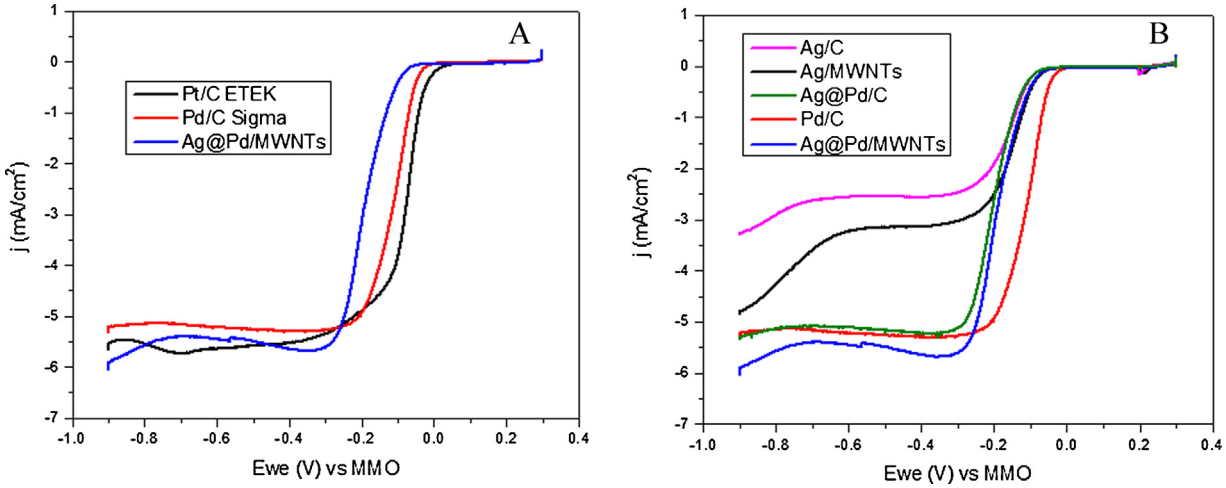

Fig. 4. A: ORR comparison of the Ag@Pd/MWNTs with standard Pt/C and Pd/C catalysts, B: ORR comparison of the core–shell catalysts, their respective precursors, and Pd/C catalysts, both graphs at 1600 rpm in 1 M KOH saturated with O_2 with a 5 mV/s scan rate.

4-electron pathways are present (Table 1). The electron transfer for the core–shell catalyst also suggests that the MWNTs are taking part in the reaction due to carbon sites following a 2-electron pathway and bulk Ag and Pd following the 4-electron pathway [30]. One possible reason for the Ag@Pd/MWNTs having a higher mass transfer limiting current density despite the less efficient ORR pathway could be due to the physical nature of the core–shell structure. The geometric strain between the two metals results in a shift of the electron band structure, which increases the activity of the catalyst and weakens the chemisorption of intermediate species [14].

3.4. ORR alcohol tolerance

To determine the effect of fuel crossover from the anode to the cathode of the fuel cell, the effect of alcohol tolerance of the catalyst was evaluated by introducing either 1 M methanol or 1 M ethanol into the electrolyte before ORR testing (Fig. 6A–D). The ideal catalyst would have the alcohol containing electrolyte curves superimposed over the non-alcohol containing electrolyte curve [20]. In the Pt/C and Pd/C curves the peaks between −0.3 and −0.2 V indicate that the alcohol is being preferentially reduced over the oxygen [20]. At −0.1 V, the current density for the Pt/C is −3.824 in 1 M KOH and −2.850 and −2.955 in 1 M KOH with the presence of 1 M MeOH and 1 M EtOH respectively (Table 2). We show a general reduction of current densities due to the presence of alcohol for Pt/C to be 0.97 (25.5% decrease) and 0.87 mA/cm^2 (22.7% decrease) and for Pd/C to be 1.09 (46.6% decrease) and 2.13 mA/cm^2 (91.2% decrease) for the methanol and ethanol respectively (Table 2). It has previously been shown that the presence of silver increases the catalyst's selectivity toward oxygen reduction over methanol [6,7]. For the Ag/MWNTs the three curves were almost the same with and without the presence of the alcohols, and is consistent with Nguyen et al. findings that showed silver is inactive toward ethanol oxidation [31]. Remarkably, the Ag@Pd/MWNTs core shell structure shows more tolerance to the presence of methanol than Ag-Pd alloys, which show preference to methanol oxidation and little ORR activity [32]. The Ag@Pd/MWNTs is equally tolerant of both methanol and ethanol present in the electrolyte. At −0.1 V the current density lowers by 0.18 mA/cm^2 (43.8% decrease) and only 0.12 mA/cm^2 (29.0% decrease) in 1 M KOH in the presence of methanol and ethanol respectively. In terms of absolute current the Ag@Pd/MWNTs have smallest decrease of only 0.12 mA/cm^2 and the Pt/C has the lowest percent decrease in current density of 25.5%. Comparing the Pd/C standard catalyst to the Ag@Pd/MWNTs, the core–shell catalyst has a smaller percent decrease and a smaller absolute decrease in current density. The onset potential negatively shifts for the Ag/MWNTs catalyst is only 7 mV for methanol and 3 mV for ethanol. For the standard catalysts, the onset potential also shifts negatively for both the Pt/C (15 mV and 39 mV) and Pd/C (71 mV and 43 mV) catalysts in both the methanol and ethanol containing electrolytes respectively. The Ag@Pd/MWNTs are the only catalyst of the four that has a positive shift of the onset potentials for both methanol (3 mV) and ethanol (8 mV). This is due to the presence of silver, which allows the palladium to selectively reduce the oxygen over methanol and does not negatively shift the onset potential of the ORR curves, which is expected because of the ensemble effects that have been previously shown in bi-metallic catalysts [4]. We show the effect of alcohol tolerance on the current density of the Ag@Pd/MWNTs and Pd/C by normalizing by the electrode surface area and the mass activity of the 2 catalysts (Fig. 6E–F). We note that to the Ag@Pd/MWNTs contains less Pd than the Pd/C, as mentioned in Section 3.1. For both the current density and mass activity, in the presence of ethanol the Ag@Pd/MWNTs have higher currents of −0.29 mA/cm^2 and −45.96 mA/mg$_{Pd}$ compared to the Pd/C of −0.21 mA/cm^2 and −8.25 mA/mg$_{Pd}$.

3.5. ORR durability

To determine the durability of the catalyst chronoamperometry measurements are conducted in O_2 saturated electrolyte at 1600 RPM and held at −0.1 V vs MMO. In Fig. 7, the durability measurements were carried out in 1 M KOH, 1 M methanol with 1 M KOH, and 1 M ethanol with 1 M KOH. At the end of 30 minute durability test the current of the Ag@Pd/MWNTs out performs the standard Pd/C in the 1 M KOH and 1 M KOH with methanol but not the ethanol containing electrolyte. However, when you compare by mass activity, the core–shell catalyst ends with −226.54 mA/mg$_{Pd}$, which is ~3.5 times the activity of the standard Pd catalyst of -65.04 mA/mg$_{Pd}$ (Table 3). The durability tests were also run for the Ag/MWNTs to compare the Ag@Pd/MWNTs to their precursor. In all three electrolytes the Ag/MWNTs are not as active a catalyst compared to the Ag@Pd/MWNTs, which further proves the increased performance of the core–shell structure. These results show that the core–shell catalyst has greater durability than the standard Pd/C catalyst and Ag/MWNT precursor, especially when the presence of alcohol may occur.

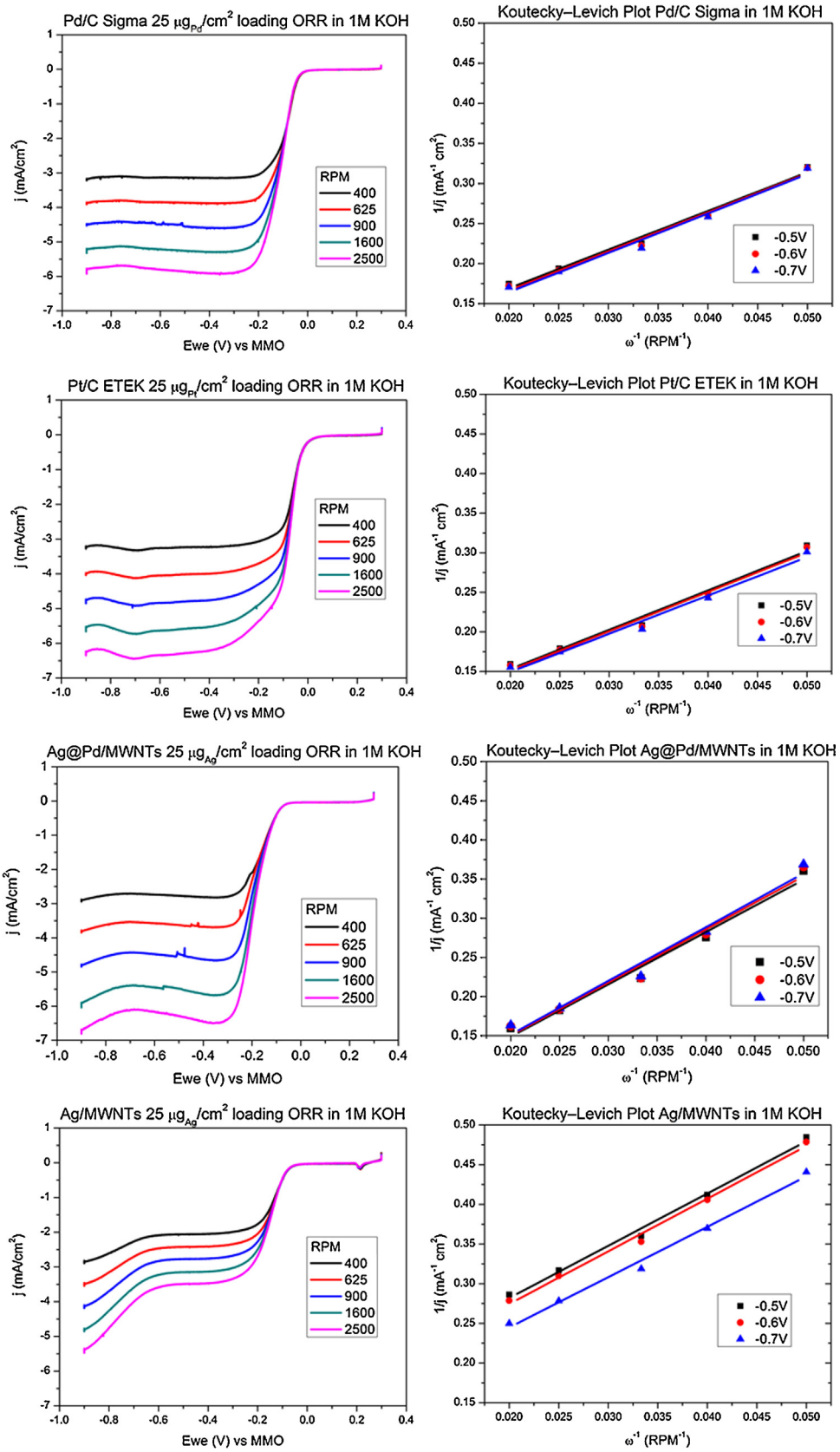

Fig. 5. Left Column- ORR curves at different RPMs, Right Column–Koutecky–Levich Plots.

Table 2
Comparison of current density, onset potential and half wave potential for the catalyst materials at 1600 RPM in different electrolytes.

	1 M KOH j @ −0.1 V (mA/cm^2)		1 M KOH 1 M MeOH		1 M KOH EtOH	
Pd/C	−2.339	−0.032	−1.250	−0.103	−0.206	−0.075
Pt/C	−3.824	0.007	−2.850	−0.008	−2.955	−0.032
Ag/MWNTs	−0.460	−0.074	−0.339	−0.081	−0.399	−0.077
Ag@Pd/MWNTs	−0.404	−0.091	−0.227	−0.088	−0.287	−0.083

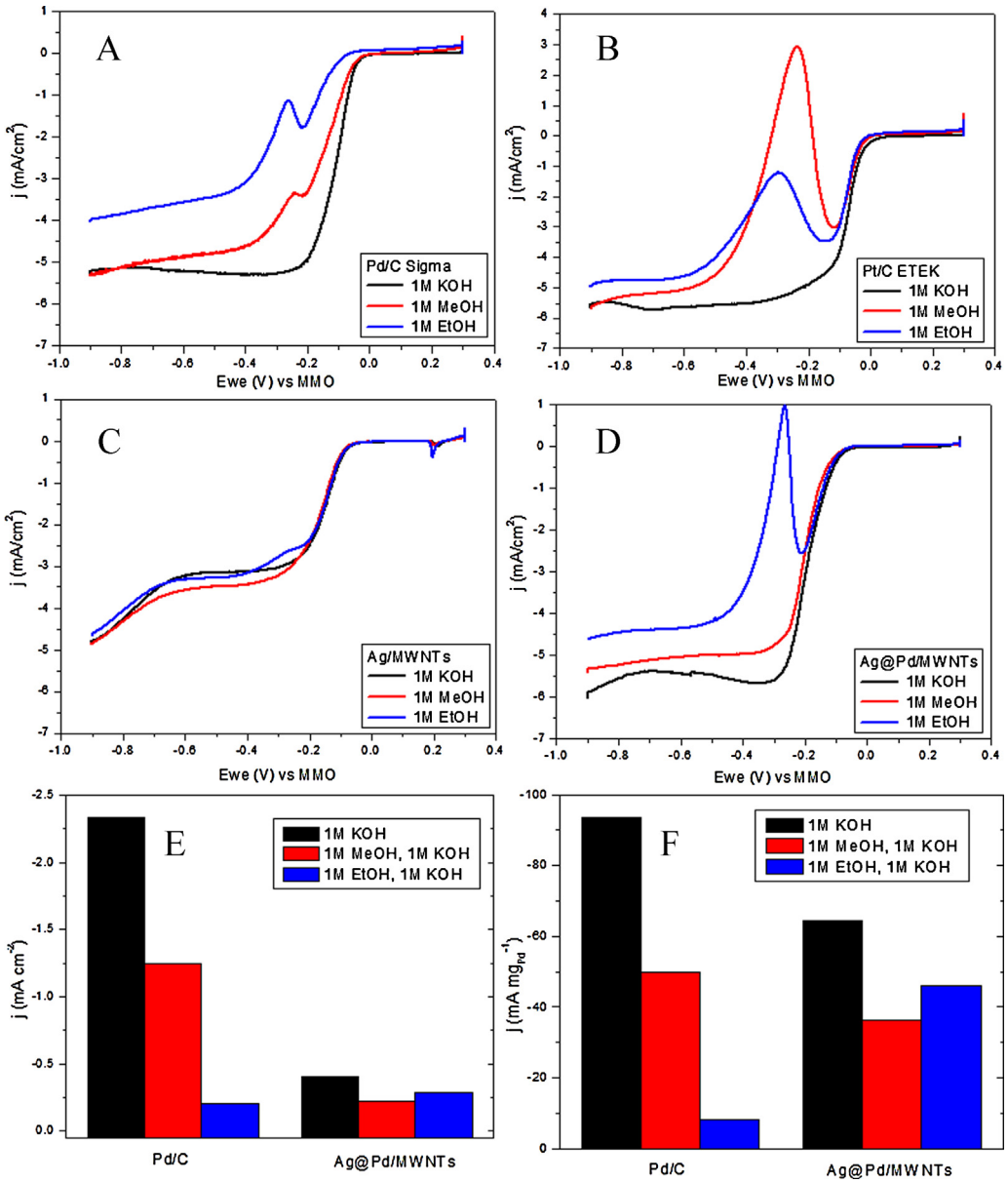

Fig. 6. (A–D) Effect of 1 M methanol or 1 M ethanol on ORR at 1600 RPM in O_2 saturated 1 M KOH, (E) Current density of Pd/C and Ag@Pd/MWNTs at −0.1 V, (F) Mass activity of Pd/C and Ag@Pd/MWNTs at −0.1 V.

Table 3
Comparison of current density and mass activity of Ag@Pd/MWNTs, Ag/MWNTs and Pd/C after durability testing, 30 min at −0.1 V in O_2 saturated electrolyte at 1600 RPM. The mass activity of the Pd containing catalysts is normalized by the mass of Pd and the Ag/MWNTs are normalized by the mass of Ag present.

	Current density (mA/cm^2)			Mass activity (mA/mg)		
	1 M KOH	1 M MeOH	1 M EtOH	1 M KOH	1 M MeOH	1 M EtOH
Ag@Pd/MWNTs	−0.98	−1.19	−1.42	−156.76	−190.69	−226.54
Pd/C	−0.86	−0.89	−1.63	−34.23	−35.43	−65.04
Ag/MWNTs	−0.31	−0.44	−0.26	−12.28	−17.45	−10.46

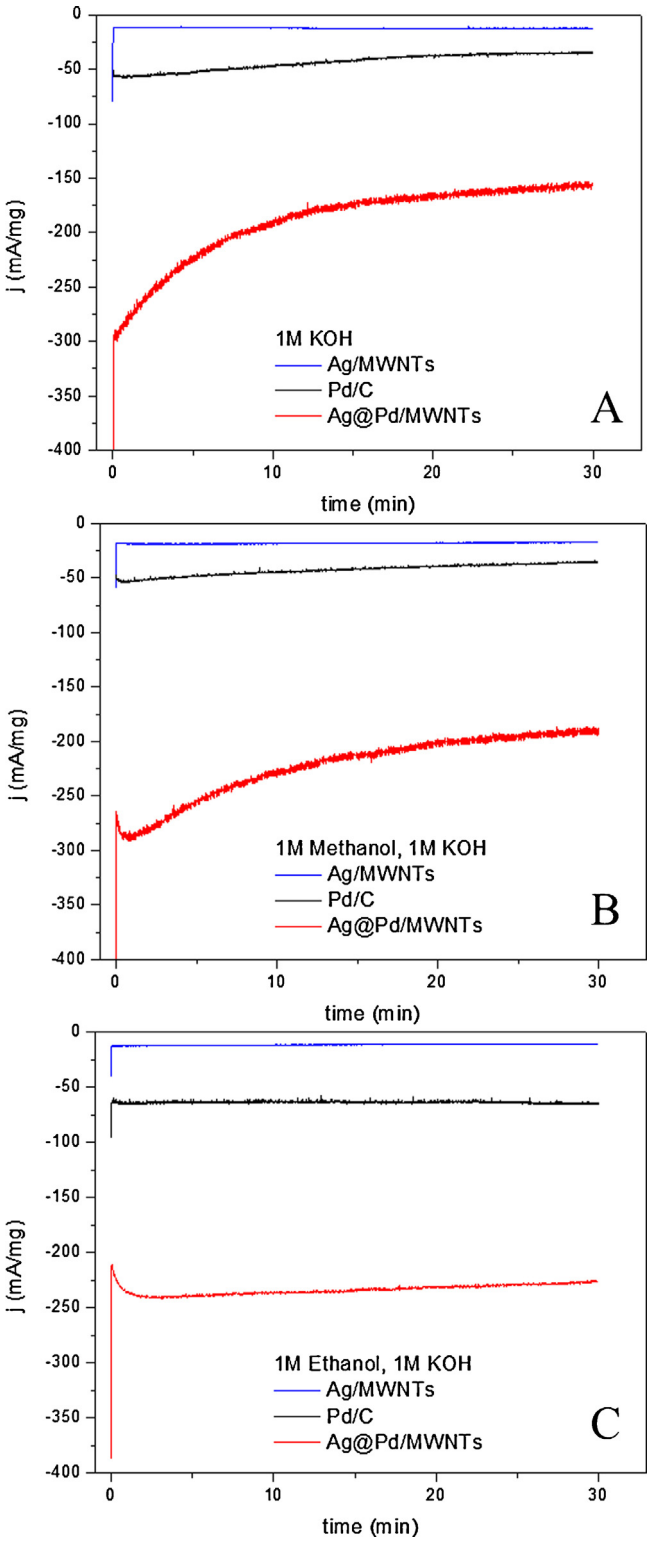

Fig. 7. Durability testing of Ag@Pd/MWNTs, Ag/MWNTs and Pd/C in O_2 saturated electrolyte at 1600 RPM, held at −0.1 V vs MMO for 30 min, reported in mass activity (mA/mg) in (A) 1 M KOH, (B) 1 M methanol and 1 M KOH, (C) 1 M ethanol and 1 M KOH.

4. Conclusion

We have successfully shown the synthesis of a Ag-Pd core–shell catalyst from galvanic displacement of Ag nanoparticles deposited on the surface of MWNTs or carbon black. It was found that the Ag@Pd/MWNTs catalyst has an average electron transfer of 3, which indicates both the 2 e^- and 4 e^- ORR pathways are present, and is similar to that of the core–shell precursor (Ag/MWNTs). Alcohol tolerance testing shows the core–shell catalyst to have higher current density for ORR in the presence of ethanol. The combined presence of silver and palladium selectively reduces oxygen over methanol and ethanol, and does not lower the onset potential of −0.09 V for the ORR curves unlike the standard Pt/C and Pd/C catalysts which are affected by the presence of alcohols. This increase in performance indicates that the physical structure of the core–shell catalyst produces an ensemble effect resulting in improved activity for ORR. The Ag@Pd/MWNTs also exhibit higher durability than the standard Pd/C catalyst. Based on these results, the best performing ORR catalyst was the Ag@Pd/MWNTs, due to its tolerance of alcohol and durability. The combination of high activity and alcohol tolerance makes the Ag@Pd/MWNTs a promising catalyst for use in direct alcohol fuel cells (DAFCs).

Acknowledgements

We gratefully acknowledge Southwest Nanotechnologies for their kind donation of the multiwalled carbon nanotubes (SWeNT® SMW100) used in this project and Dr. Helmut Ernstberger for assisting with conducting the ICP measurements. We would also like to acknowledge funding from the Yale Climate Energy Institute and the NSF-CBET-0954985 CAREER Award. Facilities use was supported by YINQE and NSF MRSEC DMR 1119826.

References

[1] X.G. Li, B.N. Popov, T. Kawahara, H. Yanagi, Journal of Power Sources 196 (2011) 1717–1722.
[2] M.C. Oliveira, R. Rego, L.S. Fernandes, P.B. Tavares, Journal of Power Sources 196 (2011) 6092–6098.
[3] M. Carmo, G. Doubek, R.C. Sekol, M. Linardi, A.D. Taylor, Journal of Power Sources 230 (2013) 169–175.
[4] C. Bianchini, P.K. Shen, Chemical Reviews 109 (2009) 4183–4206.
[5] E. Antolini, Journal of Power Sources 170 (2007) 1–12.
[6] L. Demarconnay, C. Coutanceau, J.M. Léger, Electrochimica Acta 49 (2004) 4513–4521.
[7] H. Meng, P.K. Shen, Electrochemistry Communications 8 (2006) 588–594.
[8] M. Chatenet, L. Genies-Bultel, M. Aurousseau, R. Durand, F. Andolfatto, Journal of Applied Electrochemistry 32 (2002) 1131–1140.
[9] H.-K. Lee, J.-P. Shim, M.-J. Shim, S.-W. Kim, J.-S. Lee, Materials Chemistry and Physics 45 (1996) 238–242.
[10] Y.X. Wang, P.B. Balbuena, Journal of Physical Chemistry B 109 (2005) 18902–18906.
[11] K. Sasaki, H. Naohara, Y. Cai, Y.M. Choi, P. Liu, M.B. Vukmirovic, J.X. Wang, R.R. Adzic, Angewandte Chemie International Edition 49 (2010) 8602–8607.
[12] V. Mazumder, M. Chi, K.L. More, S. Sun, Journal of the American Chemical Society 132 (2010) 7848–7849.
[13] K. Tedsree, T. Li, S. Jones, C.W.A. Chan, K.M.K. Yu, P.A.J. Bagot, E.A. Marquis, G.D.W. Smith, S.C.E. Tsang, Nature Nanotechnology 6 (2011) 302–307.
[14] P. Strasser, S. Koh, T. Anniyev, J. Greeley, K. More, C.F. Yu, Z.C. Liu, S. Kaya, D. Nordlund, H. Ogasawara, M.F. Toney, A. Nilsson, Nature Chemistry 2 (2010) 454–460.
[15] T. Bligaard, J.K. Norskov, Electrochimica Acta 52 (2007) 5512–5516.
[16] H. Kobayashi, M. Yamauchi, H. Kitagawa, Y. Kubota, K. Kato, M. Takata, Journal of the American Chemical Society 130 (2008) 1818–1819.
[17] F. Tao, M.E. Grass, Y. Zhang, D.R. Butcher, J.R. Renzas, Z. Liu, J.Y. Chung, B.S. Mun, M. Salmeron, G.A. Somorjai, Science 322 (2008) 932–934.
[18] C.F. Calver, P. Dash, R.W.J. Scott, ChemCatChem 3 (2011) 695–697.
[19] N. Khan, S. Shaikhutdinov, H. Freund, Catalysis Letters 108 (2006) 159–164.
[20] L. Jiang, A. Hsu, D. Chu, R. Chen, Electrochimica Acta 55 (2010) 4506–4511.
[21] H.T. Zheng, Y. Li, S. Chen, P.K. Shen, Journal of Power Sources 163 (2006) 371–375.
[22] M. Michel, A. Taylor, R. Sekol, P. Podsiadlo, P. Ho, N. Kotov, L. Thompson, Adv. Mater. (Weinheim, Ger.) 19 (2007) 3859–3864.
[23] A.D. Taylor, M. Michel, R.C. Sekol, J.M. Kizuka, N.A. Kotov, L.T. Thompson, Advanced Functional Materials 18 (2008), 3354-3354.
[24] G.G. Wildgoose, C.E. Banks, R.G. Compton, Small 2 (2006) 182–193.
[25] A.D. Taylor, G.J. DiLeo, K. Sun, Applied Catalysis B: Environmental 93 (2009) 126–133.
[26] Y. Lin, K.A. Watson, M.J. Fallbach, S. Ghose, J.G. Smith, D.M. Delozier, W. Cao, R.E. Crooks, J.W. Connell, ACS Nano 3 (2009) 871–884.

[27] A.D. Taylor, R.C. Sekol, J.M. Kizuka, S. D'Cunha, C.M. Comisar, Journal of Catalysis 259 (2008) 5–16.
[28] S.R. Brankovic, J.X. Wang, R.R. Adzic, Surface Science 474 (2001) L173–L179.
[29] L. Jiang, A. Hsu, D. Chu, R. Chen, Journal of The Electrochemical Society 156 (2009) B370–B376.
[30] A.C. Garcia, L.H.S. Gasparotto, J.F. Gomes, G. Tremiliosi-Filho, Electrocatalysis 3 (2012) 147–152.
[31] S.T. Nguyen, H.M. Law, H.T. Nguyen, N. Kristian, S. Wang, S.H. Chan, X. Wang, Applied Catalysis B: Environmental 91 (2009) 507–515.
[32] C.-L. Lee, H.-P. Chiou, K.-C. Chang, C.-H. Huang, International Journal of Hydrogen Energy 36 (2011) 2759–2764.